



Esophageal wound healing by aligned smooth muscle cell-laden nanofibrous patch



Miji Yeo ^{a,b,1}, Jung Won Yoon ^{c,1}, Gyu Tae Park ^c, Sung-Chan Shin ^e, Young-Cheol Song ^c, Yong-Il Cheon ^e, Byung-Joo Lee ^e, Geun Hyung Kim ^{a,d,*}, Jae Ho Kim ^{c,**}

^a Department of Biomechatronic Engineering, College of Biotechnology and Bioengineering, Sungkyunkwan University (SKKU), Suwon 16419, Republic of Korea

^b Department of Engineering Science and Mechanics, Penn State University, University Park, PA 16802, USA

^c Department of Physiology, School of Medicine, Pusan National University, Yangsan 50612, Republic of Korea

^d Biomedical Institute for Convergence at SKKU (BICS), Sungkyunkwan University, Suwon 16419, Republic of Korea

^e Department of Otorhinolaryngology-Head and Neck Surgery, College of Medicine, Pusan National University and Medical Research Institute, Pusan National University Hospital, Busan 49241, Republic of Korea

ARTICLE INFO

Keywords:

Cell electrospinning
Smooth muscle cells
Esophageal reconstruction

ABSTRACT

The esophagus exhibits peristalsis via contraction of circularly and longitudinally aligned smooth muscles, and esophageal replacement is required if there is a critical-sized wound. In this study, we proposed to reconstruct esophageal tissues using cell electrospinning (CE), an advanced technique for encapsulating living cells into fibers that allows control of the direction of fiber deposition. After treatment with transforming growth factor- β , mesenchymal stem cell-derived smooth muscle cells (SMCs) were utilized for cell electrospinning or three-dimensional bioprinting to compare the effects of aligned micropatterns on cell morphology. CE resulted in SMCs with uniaxially arranged and elongated cell morphology with upregulated expression levels of SMC-specific markers, including connexin 43, smooth muscle protein 22 alpha (SM22 α), desmin, and smothelin. When SMC-laden nanofibrous patches were transplanted into a rat esophageal defect model, the SMC patch promoted regeneration of esophageal wounds with an increased number of newly formed blood vessels and enhanced the SMC-specific markers of SM22 α and vimentin. Taken together, CE with its advantages, such as guidance of highly elongated, aligned cell morphology and accelerated SMC differentiation, can be an efficient strategy to reconstruct smooth muscle tissues and treat esophageal perforation.

1. Introduction

The esophagus is a tubular organ that extends from the epiglottis in the pharynx to the stomach. This organ is composed of thin, elongated smooth muscle cells (SMCs) aligned in a parallel manner for contractile function. When food is swallowed, the esophagus pushes the ingested food bolus toward the stomach via peristalsis, which is mediated by the contraction of circular and longitudinal esophageal muscles [1]. Esophageal diseases, such as congenital defects and esophageal cancer, cause circumferential, full-thickness, and extended segment loss of the esophagus. Gastric pull-up conduits or colon interpositions are usually used to

treat esophageal perforations. However, esophageal substitutes have shown limited success [2]. Therefore, esophageal tissue engineering has attracted attention as a promising strategy for regenerating damaged native esophagus [3]. However, to the best of our knowledge, no evidence has shown that an engineered esophageal substitute can successfully mimic the structural and functional characteristics of the smooth muscles in the esophagus. Recently, stem cell-based tissue engineering has emerged as a potential method to improve the therapeutic efficacy of engineered substitutes composed of endogenous cells.

Mesenchymal stem cells (MSCs) can differentiate into multiple cell lineages, including adipocytes, osteoblasts, chondrocytes, skeletal

* Corresponding author. Department of Biomechatronic Engineering, College of Biotechnology and Bioengineering, Sungkyunkwan University (SKKU), Suwon, 16419, Republic of Korea.

** Corresponding author.

E-mail addresses: takapy@naver.com (M. Yeo), wjddnjssky@nate.com (J.W. Yoon), daramzuy2@naver.com (G.T. Park), cha-nwi@daum.net (S.-C. Shin), dudcjf1114@naver.com (Y.-C. Song), skydragonone@naver.com (Y.-I. Cheon), voicelee@pusan.ac.kr (B.-J. Lee), gkimbme@skku.edu (G.H. Kim), jhkimst@pusan.ac.kr (J.H. Kim).

¹ These authors contributed equally to this work.

<https://doi.org/10.1016/j.mtbio.2023.100564>

Received 17 November 2022; Received in revised form 22 January 2023; Accepted 24 January 2023

Available online 26 January 2023

2590-0064/© 2023 The Authors. Published by Elsevier Ltd. This is an open access article under the CC BY-NC-ND license (<http://creativecommons.org/licenses/by-nd/4.0/>).

myocytes, and SMCs [4–6]. Transforming growth factor- β 1 (TGF- β 1) is a potent inducer of MSC-to-SMC differentiation via activation of the TGF- β -SMAD signaling cascade [7,8]. Some studies have shown that TGF- β 1 treatment increases the expression of SMC-specific ion channels in human adipose-derived MSCs [9]. In addition to extracellular stimuli, cell alignment through micropatterning has been reported to increase the expression levels of F-actin and alpha smooth muscle actin (α -SMA) in SMCs and promote the contractile phenotype [10,11]. Because direct transplantation of SMCs into damaged tissues does not support cell alignment and contractile function in smooth muscle tissues, several strategies, including the use of aligned substrates and electrospun fibers, have been developed to guide cell alignment [12,13]. However, developing an implantable substitute with an aligned pattern, mechanical strength, and bioactive cues to promote cellular activities in three dimensions (3D) remains a challenge.

Surface topography has been reported to regulate cell adhesion, cytoskeletal organization, and cell-cell interactions and plays a key role in the lineage specification of stem cells [14,15]. Cells sense surface patterns and nanoscale biochemical and biophysical stimuli [16]; sub-micron topography regulates various stem cell responses, including proliferation, migration, and differentiation [17] by changing the focal adhesion assembly, which causes variations in cytoskeletal organization and cell mechanical properties [18]. Therefore, topographical features, such as anisotropic patterning, nanostructures, and fibrillar structures, could play a significant role in spatial organization during myogenesis [19–21]. Microgrooved topography with stiff substrates has been shown to stimulate differentiation of MSCs into SMCs [22]. Moreover, micro-grooved topography and TGF- β 1 treatment synergistically stimulate the expression of SMC-specific contractile proteins in MSCs [23]. However, topographic modulation in esophageal tissue engineering using MSCs has not yet been studied.

3D cell printing (CP) is an emerging technique for fabricating tissue substitutes that can mimic tissues or organs, but generating a 3D construct with tissue-specific cells and desired topographic features has been challenging [24,25]. Electrospinning is a prevailing technique generating micro/nanofibers using both synthetic and natural polymers. Allowing reconstruction of desired topographic features, electrospinning has been utilized for various applications, including smart materials (i.e., stimuli-responsive mats, superhydrophilic or superhydrophobic mats, and sensors), environmentally friendly materials (i.e., membranes for water and air filtration), soft electronics (i.e., flexible and stretchable materials and personal devices), and biomedical applications (i.e., nanofiber-based scaffolds with biophysical and biochemical cues) [26,27]. Cell electrospinning (CE) has great potential in biomedical applications due to its ability to encapsulate living cells directly into micro-/nanofibers while allowing the control of micropattern formation. This process improves nutritional accessibility and cell distribution at different scales of the scaffold, which can overcome the limitations of conventional electrospinning and 3D bioprinting techniques [28]. Owing to CE advantages, various cell types, such as neuroblastoma cells, cardiac myocytes, osteoblasts, and adipose stem cells, have been utilized in CE [28–31]. In addition, we previously demonstrated that myoblasts and human umbilical vein endothelial cells could be successfully remodeled into an aligned topography using the CE process [32,33]. Hence, in this study, CE was utilized to build an anisotropically arranged smooth muscle substitute to mimic native esophageal tissues.

As of now, there have been several attempts to develop engineered esophageal substitutes. For instance, electrospinning was utilized using the mixture of decellularized esophagus extracellular matrix (ECM) and polyamide-6 (PA-6) [34]. Human adipose- and bone marrow-derived mesenchymal stromal cells were cultured on randomly oriented ECM/PA-6 fibers, in which some cell proliferation was revealed with 25% of scaffold cell coverage. On the other hand, electro-hydrodynamic jetting was carried out using the blend of polycaprolactone (PCL) and Pluronic F127 (PF127) to develop scaffolds in 90° grid patterns [35]. PCL/PF127 scaffolds showed an enhanced ultimate tensile strength (1.2

MPa) by PCL and better wettability by PF127. Further, when human esophageal fibroblasts were cultured on the PCL/PF127 scaffold, cell growth direction was guided *in vitro* by the orientation of scaffolds in two perpendicular directions. These studies have shown potential of *in vitro* engineered esophageal scaffolds, but acellular fabrication techniques eventually cause inhomogeneous cell distribution by cell seeding and include multiple fabrication steps increasing risks of external contamination factors prior to implantation. Also, differentiation to esophageal smooth muscle cells and *in vivo* study should be more thoroughly investigated to further verify healing capacity as esophageal substitutes.

In this study, several main driving factors of SMC regeneration were investigated to validate the CE process. Briefly, MSCs and TGF- β 1-treated MSCs (referred to as SMCs) were compared using SMC-specific markers to estimate the efficiency of MSC-to-SMC differentiation. Followed by TGF- β 1 treatment, MSCs and SMCs were cultured on a 2D substrate with and without aligned electrospun fibers to estimate the effects on cell alignment and SMC differentiation. Finally, MSCs and SMCs were utilized to develop a cell-laden 3D substitute fabricated via CE and CP and examined for various cellular activities. To assess the applicability of CE in clinical use, we developed an aligned SMC-laden fibrous patch and examined its therapeutic effects using a rat esophageal wound model.

2. Materials & methods

2.1. Materials

α -Minimum Essential Medium (α -MEM), Hank's balanced salt solution (HBSS), fetal bovine serum (FBS), and trypsin-EDTA were purchased from Invitrogen (Carlsbad, CA, USA). TGF- β 1 was purchased from PeproTech (Cranbury, NJ, USA). Smooth muscle growth medium-2 (SmGMTM-2) was purchased from Lonza (Bazel, Switzerland). Polycaprolactone (PCL; molecular weight (M_w) = 45,000 Da), calcium chloride ($CaCl_2$), and polyethylene oxide (PEO; M_w = 900,000) were purchased from Sigma-Aldrich (St. Louis, MO, USA). Sodium alginate with 0.42 mannuronic acid to guluronic acid (M/G) ratio (LF10/60; FMC Biopolymer, Drammen, Norway) was kindly provided by Pharmaline (Suwon, South Korea). 4',6-diamidino-2-phenylindole (DAPI) was purchased from Merck (Darmstadt, Germany). The antibodies used in this study are listed in Table S1.

2.2. Culture of MSCs and differentiation to SMCs

After obtaining informed consent from patients, human palatine tonsil tissues were isolated from patients undergoing tonsillectomy for chronic tonsillar hypertrophy and chronic tonsillitis in the Department of Otorhinolaryngology-Head and Neck Surgery, Pusan National University Hospital [36,37]. To isolate tonsil-derived MSCs, tonsil tissues were washed with phosphate-buffered saline (PBS) and digested at 37 °C for 30 min with 0.075% type I collagenase. The enzyme activity was neutralized with α -MEM supplemented with 10% FBS and 10% penicillin-streptomycin. The dissociated cells were filtered through a sterile 70 μ m cell strainer and cultured in 5% CO₂ at 37 °C. When the cell confluence reached 70–80%, the cells were washed twice with HBSS, treated with 0.05% trypsin-EDTA, and incubated in 5% CO₂ at 37 °C for 3–5 min. The suspended cells were harvested in medium containing FBS and centrifuged at 500×g for 4 min. MSCs were subcultured at a split ratio of 1:3 or 1:4, and cells at passage 7–9 were used for experiments. To differentiate MSCs into SMCs, MSCs were serum-starved in α -MEM basal medium for 24 h, treated with 2 ng/mL TGF- β 1 for 4 days, and then maintained in SmGMTM-2 medium. The expression of SMC markers was determined by western blotting and flow cytometric analysis.

2.3. Western blotting

To extract total proteins, cells were treated with lysis buffer (20 mM Tris-HCl, 1 mM EGTA, 1 mM EDTA, 10 mM NaCl, 0.1 mM

phenylmethylsulfonyl fluoride, 1 mM Na₃VO₄, 30 mM sodium pyrophosphate, 25 mM β-glycerol phosphate, and 1% Triton X-100, pH 7.4), followed by sonication and centrifugation at 12,000 rpm at 4 °C for 10 min. Lysates were resolved using sodium dodecyl sulfate-polyacrylamide gel electrophoresis and transferred onto nitrocellulose membranes. The membranes were blocked with 5% skim milk buffer for 2 h and incubated overnight with primary antibodies. For visualization with chemiluminescence, the membranes were incubated with horseradish peroxidase-conjugated secondary antibodies for 1 h, and the signal was detected using an ECL kit (Cytiva, Mariborough, MA, USA). The membrane was washed four times for 20 min with 1 × Tris-buffered saline with Tween 20.

2.4. Flow cytometric analysis

MSCs and MSC-derived SMCs were fixed with 4% paraformaldehyde (PFA) for 1 h at 4 °C, and washed with PBS three times. The cells were permeabilized with 0.1% triton X-100 for 30 min and blocked with 0.5% BSA for 1 h. Primary antibodies were incubated with cells at 4 °C for 1 h, and the cells were treated with secondary antibodies conjugated with Alexa Fluor 647 (Invitrogen) at 4 °C for 30 min. Cells labeled with fluorescent antibodies were washed with PBS three times and analyzed by Attune NxT Flow cytometer (Thermofisher, USA). Obtained fluorescence signals were analyzed using the FlowJo (ver 10, Tree Star Inc.).

2.5. Cell growth on two-dimensional (2D) surface with or without aligned fibers

A rectangular glass (10 × 10 mm) was used as the non-fibrous surface. Aligned alginate fibers were deposited by electrospinning onto the glass under a 10.5 kV high-voltage power source, 140 mm nozzle-to-electrode (NtE) distance, 0.25 mL/h flow rate, and 3 min of electrospinning time. The fibers were aligned using rectangular copper electrodes (75 × 25 mm) and a metal nozzle (180 μm inner diameter). MSCs and SMCs were diluted to 62,500 cells/droplet and the equivalent number of cells laden on the CE scaffold were seeded onto the glass with or without aligned fibers.

2.6. Preparation of cell-laden bioink

To prepare the cell-laden bioink, 20 mg/mL alginate and 30 mg/mL PEO (A2P3) were dissolved in triple-distilled water and magnetically stirred for 2 days at 4 °C. Then, 1 × 10⁷ cells/mL MSCs or SMCs were added to the A2P3 solution.

2.7. Fabrication of cell-printed and cell-electrospun scaffolds using MSCs and SMCs

A 3D printer (DTR3-2210-T-SG, DASA Robot, Bucheon, South Korea) was used to fabricate the PCL strut (300 μm in diameter and 30 mm in length). Pneumatic pressure (340 kPa) was applied to the heated metal barrel containing PCL at 100 °C, and the melted PCL was extruded through a metal nozzle (350 μm inner diameter) at 10 mm/s. Subsequently, CP was performed on the printed PCL struts. The cell-laden bioink was printed through a nozzle (180 μm inner diameter) using a pneumatic pressure of 120 kPa and nozzle moving speed of 10 mm/s.

For CE, a high-voltage power source (SHV300RD-50K, Convertech, Gwangmyeong, South Korea) and syringe pump (KDS 230, NanoNC, Inc., Seoul, South Korea) were prepared. The cell-laden bioink was supplied at 0.25 mL/h, and electrospun under a 10.5 kV high voltage direct current (HVDC) and 140 mm NtE distance. Electrospun fibers were deposited on the PCL strut, which was fixed between parallel cylindrical electrodes at a distance of 30 mm.

To fabricate the PCL fibrous mat, electrospinning was performed using 10% PCL dissolved in methylene chloride and dimethylformamide at a ratio of 4:1. The PCL fibers were collected on a grounded rotating

drum at 1500 rpm using 0.20 mL/h flow rate and 0.1 kV/mm electric field (12 kV HVDC and 120 mm NtE distance) for 4 h.

2.8. In vitro characterization

Optical images were captured using a BX FM-32 optical microscope (Olympus, Japan) to observe the surface topography of the constructs. To obtain microscale images, the samples were placed on double-sided carbon tape and sputter-coated with gold, and their images were captured using a scanning electron microscope (SEM; SNE-3000 M; SEC Inc., Suwon, South Korea).

Stress-strain curves were obtained using a microtensile tester (Top-tech 2000; Chemilab, Suwon, South Korea) under uniaxial stretching at 0.2 mm/s. The samples were vertically fixed between two grips with a 10 mm gap and stretched upward until failure.

2.9. Analysis of cell viability and differentiation on cell-laden scaffolds

Cell viability at various time points during culturing (days 0, 7, 14, and 21) was measured using a Live/Dead Viability/Cytotoxicity Kit (Invitrogen). The samples were immersed in a solution containing 0.15 mM calcine AM and 2 mM ethidium homodimer-1 for 30 min, and images were captured using a light microscope. Cell viability was calculated as the ratio of the number of live cells to the total cell number using Fiji software.

Cell nuclei and F-actin were visualized by DAPI (blue) and phalloidin (green) staining, respectively. The samples were fixed in formaldehyde solution (3.7% in Tris-buffered saline [TBS]) for 12 h at 4 °C and treated with 0.3% Triton X-100 in TBS for 10 min at 25 °C. The samples were then treated for 1 h at 37 °C with a solution of phalloidin (15 U/mL; Invitrogen) and DAPI (5 μM; Invitrogen). Fluorescence images were captured using a confocal microscope (LSM 700; Carl Zeiss, Germany) and analyzed using Fiji software.

Differentiation of MSCs and SMCs was observed using immunofluorescence staining. The samples were fixed and permeabilized prior to phalloidin and DAPI staining. The samples were then immersed in 1% bovine serum albumin in TBS for 1 h at room temperature. Primary antibodies against α-SMA, fibronectin, calponin, collagen I, and collagen IV at a 1:200 dilution in TBS were added to the samples and incubated overnight at 4 °C. The samples were subsequently stained with secondary antibodies conjugated with Alexa Fluor 488 or 594 (Invitrogen). Images were captured using confocal microscopy and analyzed using Fiji software.

2.10. Reverse transcription-quantitative polymerase chain reaction (RT-qPCR)

The expression levels of connexin 43 (CX43), smooth muscle protein 22 alpha (SM22α), desmin, and smoothelin (SMTN) were analyzed by RT-qPCR. Briefly, total RNA was isolated using TRI reagent (Sigma-Aldrich), according to the manufacturer's instructions. The purity and concentration of the isolated RNA were determined using a spectrophotometer (FLX800T; Bioteck, VT, USA). cDNA synthesis was performed using 500 ng RNase-free, DNase-treated, total RNA using a reverse transcription system (FSQ-201; Toyobo, Osaka, Japan). Gene expression levels were measured by the comparative C_t method using the StepOne Plus RT-PCR system (Applied Biosystems, Foster City, CA, USA). GAPDH expression was used as an internal control. The primers used in this study are listed in Table S2.

2.11. Repair of esophageal wounds using SMC-laden patch

Six-month-old Sprague-Dawley rats (Central Lab Animal Inc., Seoul, Korea), weighing approximately 680–700 g, were used in this study. The rats were divided into three groups (n = 3 per group) and anesthetized with isoflurane (Baxter International Inc., USA). Two independent

animal experiments were repeated for statistical analysis of histological and immunostaining results. Anesthesia delivery equipment was used to administer a gas mixture of isoflurane and O₂ via inhalation into the rat's respiratory system. Before anesthesia, isoflurane was evaporated in a vaporizer (Harvard Apparatus, USA), and the concentration was set to 5% and adjusted to 2% during the operation. The gas flow rate of O₂ was maintained at 0.5–1 L/min.

To create the esophageal wound model, the center of the ventral neck was shaved, an incision of approximately 2 cm was made, and the esophagus was located in the tracheoesophageal structure. To equalize the size of the esophageal wound, a 2 mm diameter biopsy punch (Miltex, KAI Industries, Japan) was used to completely puncture the muscle and mucosal layer of the esophagus. The patches were cut with a 4 mm diameter biopsy punch and placed over the esophageal wound, and the punctured section of the esophagus was sutured with a 9–0 nylon suture (AILEE Co., Korea). The incised skin was sutured using a 7–0 nylon suture. All surgical procedures were performed using sterile instruments and disinfection procedures. The mice were fasted for the first 3 days, sterilized water was provided after 4 days, and food was provided after 6 days, postoperatively. During the fasting period, the water consumption was considered as evidence of esophageal restoration. Two weeks after surgery, the rats were sacrificed by CO₂ euthanasia. All animal experiments were reviewed and approved by the Institutional Review Board of the Pusan National University Hospital (PNUH-2021-188).

2.12. Histological analysis

For histological analysis of esophageal regeneration, esophageal tissues were excised along with tracheal tissue to support the esophagus. For routine staining, tissues were fixed with cooled acetone. To obtain cryosections, the tissue was perfused with sucrose solution, embedded in optimal cutting temperature compound, and frozen at –80 °C. Tissue sections were then stained with hematoxylin and eosin (H&E) and Masson's trichrome stain. Stained sections were scanned using an Axio Scan.Z1 (Carl Zeiss Microscopy).

For immunohistochemical analysis, the tissue samples were fixed in 4% PFAPFA overnight and embedded in paraffin. To detect smooth muscle regeneration and vascularization, the esophageal tissue sections were stained with anti-SM22α, anti-IL-B4, anti-vimentin, and anti-desmin antibodies. Epithelium of esophageal tissues were stained with anti-cytokeratin 14, and Macrophages were stained with anti-CD68 antibody. The secondary antibodies used were goat anti-mouse antibody conjugated with Alexa Fluor 488 or 568 and streptavidin conjugated to Alexa Fluor 488, and DAPI was used to stain the nuclei. The stained sections were visualized under a laser confocal microscope (Olympus Fluoview FV1000) and an Axio Scan.Z1 (Carl Zeiss Microscopy). The fluorescence levels were quantified in a high-power field using ImageJ software.

2.13. Statistical analysis

The data are presented as the mean ± standard deviation and were analyzed using SPSS 18 software (SPSS, Inc., Chicago, IL, USA). Differences among multiple groups were compared by one-way ANOVA with post-hoc Bonferroni tests, and statistical significance was represented as *p < 0.05, **p < 0.01, and ***p < 0.001.

3. Results

3.1. MSC-to-SMC differentiation via TGF-β1 treatment and surface topography

Prior to applying CE or CP, differentiation of MSCs into SMCs *in vitro* was induced by treating MSCs with TGF-β1, and its efficacy was analyzed using western blotting. TGF-β1 treatment increased the expression levels of several SMC markers, including calponin, α-SMA, SM22α, vimentin,

desmin, and SMTN, indicating that MSCs had successfully differentiated into SMCs (Fig. S1). To confirm the TGF-β1-induced differentiation of MSCs to SMCs, the expression of SMC markers, such as α-SMA and SM22α, were measured by flow cytometric analysis. The expression levels of α-SMA and SM22α were greatly increased in SMCs compared with MSCs, and the percentages of α-SMA- and SM22α-positive cells in SMCs were 93.4% and 84.6%, respectively (Fig. S1b). In addition, phosphorylation levels of Smad2, which is a key transcription factor involved in TGF-β signaling, was elevated in SMCs than MSCs (Fig. S1c), indicating pivotal role of Smad2 in the TGF-β1-induced differentiation of MSCs to SMCs.

The effects of the aligned topography on SMC differentiation were examined in 2D cultures. It has been reported that cell elongation promotes the differentiation of MSCs into SMCs [12,38], and cell morphologies affect the phenotypic modulation of SMCs [39]. MSCs and SMCs were seeded after electrospinning the aligned fibers on a 2D substrate (Fig. S2a). A plain 2D substrate was used as a control. Compared to the cells cultured on the plain surface, the MSCs and SMCs cultured on the aligned fibers exhibited higher degrees of cell elongation and cell alignment as well as increased expression levels of SMC markers (α-SMA and calponin) and SMC-related extracellular matrix (ECM) markers (collagen I, collagen IV, and fibronectin) (Figs. S2b–d). These results suggest that the differentiation of MSCs into SMCs was promoted by cell alignment and elongation in 2D. Thus, MSCs and SMCs were used in CE to obtain aligned fibers and develop a smooth muscle regenerative scaffold.

3.2. CP and CE of MSCs and SMCs

Next, we compared the effects of CE and CP in the presence of cell alignment. The bioink was prepared by mixing a 2% alginate and 3% PEO (A2P3) solution with MSCs and SMCs at 1 × 10⁷ cells/mL. Alginate is a biocompatible, non-toxic, and versatile polymer that enables rapid gelation of the microstructure through the addition of cations [40]. PEO was added as a processing material to optimize the surface tension, conductivity, and molecular entanglement for electrospinning [41]. The composition of the A2P3 solution was based on a previous study that showed stable fiber formation and alignment [32]. As shown in Fig. 1a, CP and CE were performed with SMC-laden A2P3, according to the schematic illustration. In the optical images, a cell-electrospun scaffold had an aligned fibrous structure, whereas the cell-printed scaffold had a plain bulk structure. The morphology of SMCs was observed by phalloidin/DAPI staining after 7 days of culture. The cells of the CP scaffold had a round shape similar to that on day 0, whereas the cells of the CE scaffold exhibited an elongated morphology. These results clearly showed different degrees of cell alignment and elongation, depending on the presence of aligned micropatterns in a 3D environment. However, these scaffolds, which can be easily bent and deformed, are unsuitable for long-term culture because of their low mechanical strength.

To supplement the low mechanical strength of the electrospun or bioprinted structures, a PCL strut was applied as a mechanical support for the CP and CE processes. To generate PCL struts, PCL pellets were melted at a high temperature of 100 °C and then 3D printed using 340 kPa of pneumatic pressure and 10 mm/s nozzle moving speed, yielding a 300 μm PCL strut (Fig. 1b (i)). Then, using CP, MSCs and SMCs were printed onto the PCL strut using 120 kPa of pneumatic pressure and 10 mm/s nozzle moving speed, which are referred to as CP-MSC and CP-SMC, respectively (Fig. 1b (ii)). In the meantime, CE using MSCs and SMCs was performed on the PCL strut with fabricating parameters of 140 mm NtE distance, 0.075 kV/mm electric field, and 0.25 mL/h flow rate (Fig. 1b (iii)). The scaffolds created by CE using MSCs and SMCs are referred to as CE-MSC and CE-SMC, respectively.

The topographical features of the scaffolds fabricated using CP and CE were captured using optical and SEM imaging. The CP scaffolds exhibited plain surfaces, whereas the CE fibers exhibited aligned micropatterns (Fig. 1c and d). When MSCs were utilized for both CP and CE process,

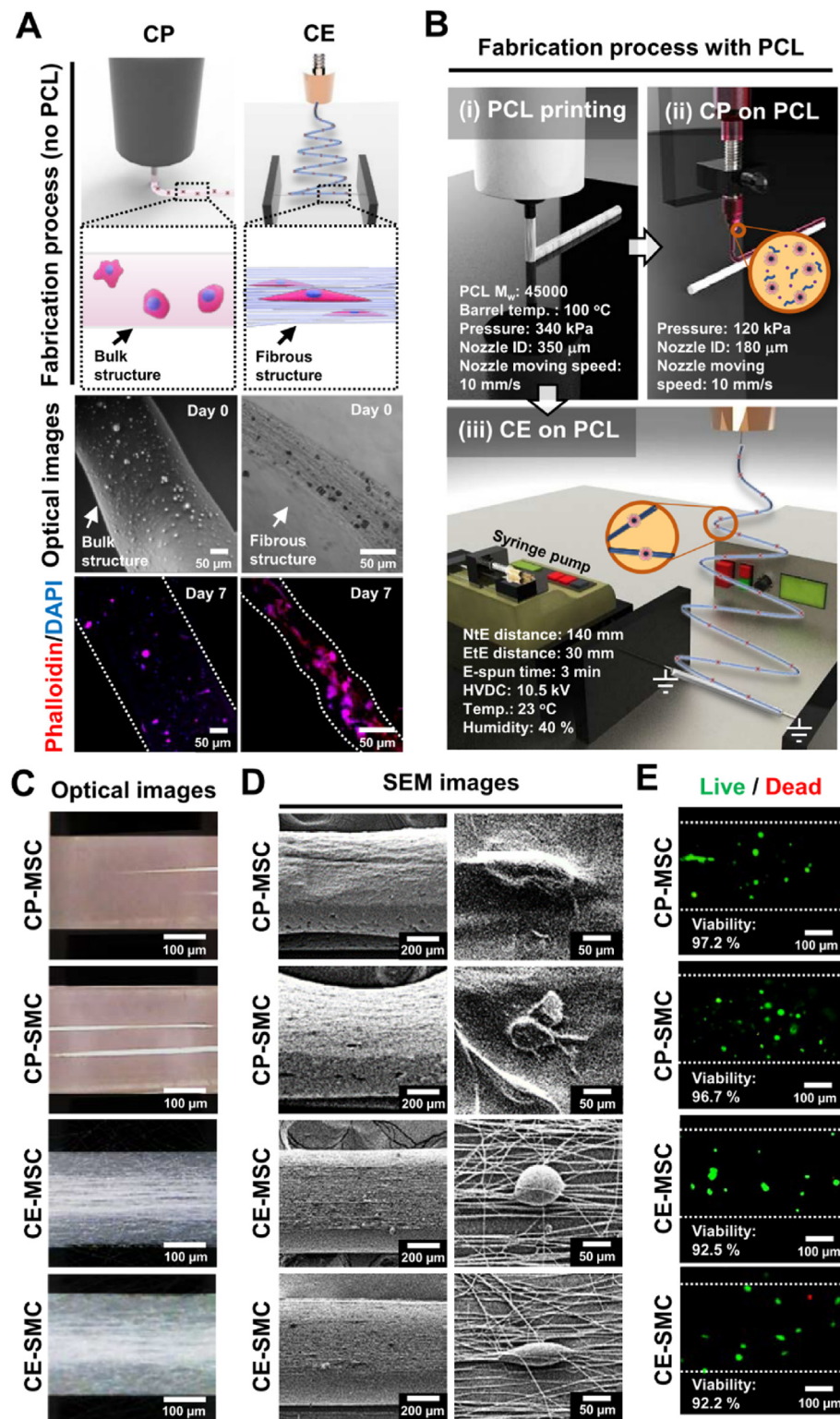


Fig. 1. Microstructures of cell printing (CP) and cell electrospinning (CE) with mesenchymal stem cells (MSCs) and stem cell-derived smooth muscle cells (SMCs). (a) Schematic illustration of CP and CE process without the supplement of a polycaprolactone (PCL) strut. The fabrication procedures for CE and CP are shown in the upper panels, and the optical and fluorescent images (phalloidin/DAPI double staining) were captured on days 0 and 7. (b) A schematic illustration of the PCL printing, CP, and CE processes. The fabricated scaffolds (CP-MSC, CP-SMC, CE-MSC, and CE-SMC) are represented as (c) optical, (d) SEM, and (e) live/dead cell images on day 0.

MSC-laden scaffolds in the absence of TGF- β 1 treatment show the effects of aligned micropatterns on SMC differentiation. To evaluate the biocompatibility of the CP and CE processes, the viability of the MSCs and SMCs on each scaffold was measured. The results showed high initial cell viability (>90%) for MSC- and SMC-laden scaffolds (Fig. 1e), indicating that both CP and CE structures provided a biocompatible microenvironment for MSCs and SMCs.

3.3. Cell compatibility of cell-printed and cell-electrospun scaffolds

Fig. 2a shows the cell viability after the CP and CE processes, in which live (green) and dead (red) cells were captured after 7, 14, and 21 days of culturing. High cell viability over 90% was maintained for 21 days for the MSCs and SMCs, indicating that both the CP and CE processes provided the cells with a biocompatible microenvironment to support cellular activities (Fig. 2b). Next, the number of cells on day 21 was counted from

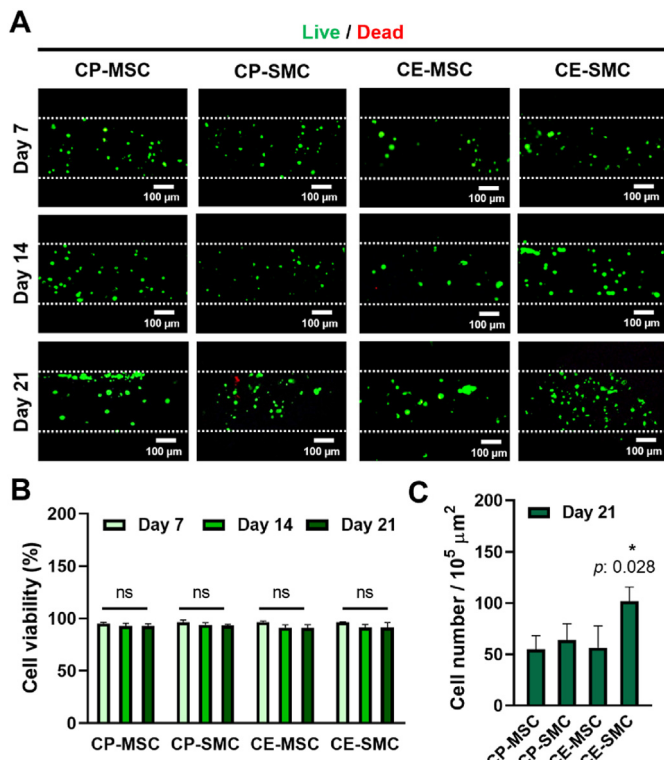


Fig. 2. Biocompatibility of cell printing (CP) and cell electrospinning (CE) represented by cell viability and the number of cells. (a) Live/Dead images of CP-mesenchymal stem cell (MSC), CP-stem cell-derived smooth muscle cell (SMC), CE-MSC, and CE-SMC on days 7, 14, and 21. Quantification of the Live/Dead images with respect to (b) cell viability and (c) cell numbers. Data indicate mean \pm SD ($n = 5$).

the images of the Live/Dead assay (Fig. 2c). CE-SMC showed the highest cell numbers compared to the other groups, suggesting that cell proliferation was promoted by the synergistic effects of TGF- β [42] and the submicron structure that are favorable for cell migration and nutrient exchange.

3.4. Effects of CP and CE on SMC differentiation

Fig. 3a shows DAPI/phalloidin staining of MSCs and SMCs on the CP and CE scaffolds. The CP scaffolds (CP-MSC and CP-SMC) contained cells with multipolar morphology, while the CE scaffolds (CE-MSC and CE-SMC) had anisotropically aligned, spindle-shaped cells. These features were quantitatively analyzed using the F-actin aspect ratio and orientation (Fig. 3b and c). The non-elongated and randomly oriented morphology of cells on the CP scaffolds had lower F-actin aspect ratios and orientation factor, while these factors were greatly increased in cells on the CE scaffolds. Furthermore, ECM components, such as fibronectin, collagen I, and collagen IV, were shown to form cytoskeletal structures (Fig. 3d). Fibronectin has been reported to enhance cell migration [43], and collagen has been shown to enhance mechanical strength and prevent physical failure of tissues [44]. CE-SMCs showed enhanced expression of all three ECM components (fibronectin, collagen I, and collagen IV) (Fig. 3e).

α -SMA is an actin isoform developed to contribute to cell-generated mechanical tension and can be used as a marker of early stage SMC differentiation [45]. Despite having a well-developed cytoskeletal structure, CP-MSCs and CE-MSCs showed very low expression of α -SMA (Fig. 4a). The expression levels and aspect ratio of α -SMA in CP-SMCs and CE-SMCs were upregulated 3-fold compared to those in MSCs (Fig. 4b). Additionally, the α -SMA orientation factor was significantly higher in

CP-MSCs and CE-MSCs owing to the cell arrangement along the aligned topographical cues (Fig. 4c). Calponin, a smooth muscle-specific protein expressed during the later stages of differentiation, was used to measure the degree of SMC differentiation. Significantly higher calponin expression was observed in SMCs than that in MSCs (Fig. 4d), suggesting that cells treated with TGF- β (SMC-laden scaffolds) could successfully initiate SMC differentiation, while cells without TGF- β treatment (MSC-laden scaffolds) may not fully differentiate into SMCs. Then, the levels of smooth muscle-specific genes were evaluated by qPCR analysis (Fig. 4e). The expression levels of CX43, SM22 α , desmin, and SMTN were highest in CE-SMCs compared to those in the other groups, suggesting that CE-SMCs exhibited more mature SMC phenotypes.

3.5. Development of a cell-laden patch using PCL fibrous mat for transplantation

Prior to *in vivo* application, a solid PCL strut was used as a mechanical support for the *in vitro* study; however, this solid structure would not be suitable for transplantation onto the curved surface of the esophagus. Therefore, the PCL strut was substituted with acellular, flexible PCL fibers fabricated via electrospinning (Fig. S3a). Here, PCL fibers were deposited in aligned patterns, and random patterns were not considered for comparison. Indeed, CP scaffold is rational as a control group to be consistent with *in vitro* test. However, SMCs on CP scaffold will get more affected by micropattern of PCL fibrous mat instead of bulky, non-patterned printed structure, so the experimental groups were opted to show effects of aligned micropattern and electrospun SMCs. Furthermore, since PCL provides high biocompatibility, strong mechanical integrity, and slow degradation rate suitable for *in vivo* tests [46], it was selected to fabricate a fibrous mat. Moreover, alginate nanofibers ($0.7 \pm 0.3 \mu\text{m}$), specifically less than $1 \mu\text{m}$ diameter, may not provide surface area sufficient for cell proliferation, but PCL microfibers ($1.1 \pm 0.2 \mu\text{m}$) can support cell adhesion, viability, and proliferation [47,48]. In the meantime, PCL fiber density was found to not affect cell proliferation rate significantly [46]. The PCL fibers were then compared with PCL struts and alginate fibers, which exhibited much stiffer mechanical properties, as shown in the stress-strain curves (Fig. S3b). In addition, Young's modulus values (1.7 ± 0.2 and $2.0 \pm 0.1 \text{ MPa}$) and maximum strength (8.6 ± 2.5 and $9.2 \pm 1.7 \text{ MPa}$) were similar between PCL fibers and PCL struts (Fig. S3c). Owing to its flexible shape and appropriate mechanical properties, a PCL fibrous mat was used to develop a cell-laden structure for *in vivo* testing.

3.6. Regeneration of esophageal wound using electrospun SMC patch *in vivo*

Esophageal replacement is often required by patients with esophageal diseases; therefore, engineered esophageal substitutes must be verified for their feasibility and regenerative effects [49]. Among the different methods investigated *in vitro*, CE-SMC exhibited more mature SMC-like phenotypes; therefore, it was selected to study the therapeutic effects in an *in vivo* esophageal wound model. An acellular PCL patch was used as a control.

The esophagus is composed of inner and outer muscle layers, arranged in circular and longitudinal orientations, respectively. To fabricate a patch for esophageal transplantation, PCL was first electrospun onto a drum collector to produce a PCL fibrous mat (Fig. 5a). To mimic the structure of the esophagus, SMCs were electrospun in five layers in the horizontal and vertical directions and cultured for 4 weeks prior to transplantation. For transplantation, the fabricated patch was shaped with a 4 mm diameter biopsy punch (Fig. 5b (i)). To generate the rat esophageal wound model, the esophageal tissue was punctured with a 2 mm biopsy punch (Fig. 5b (ii)), and the muscles around the esophagus and the inner mucosal layer were completely removed (Fig. 5b (iii), (iv)). Subsequently, the punctured section of the esophagus was covered with the fabricated patch and sutured (Fig. 5b (v)). Two weeks after surgery,

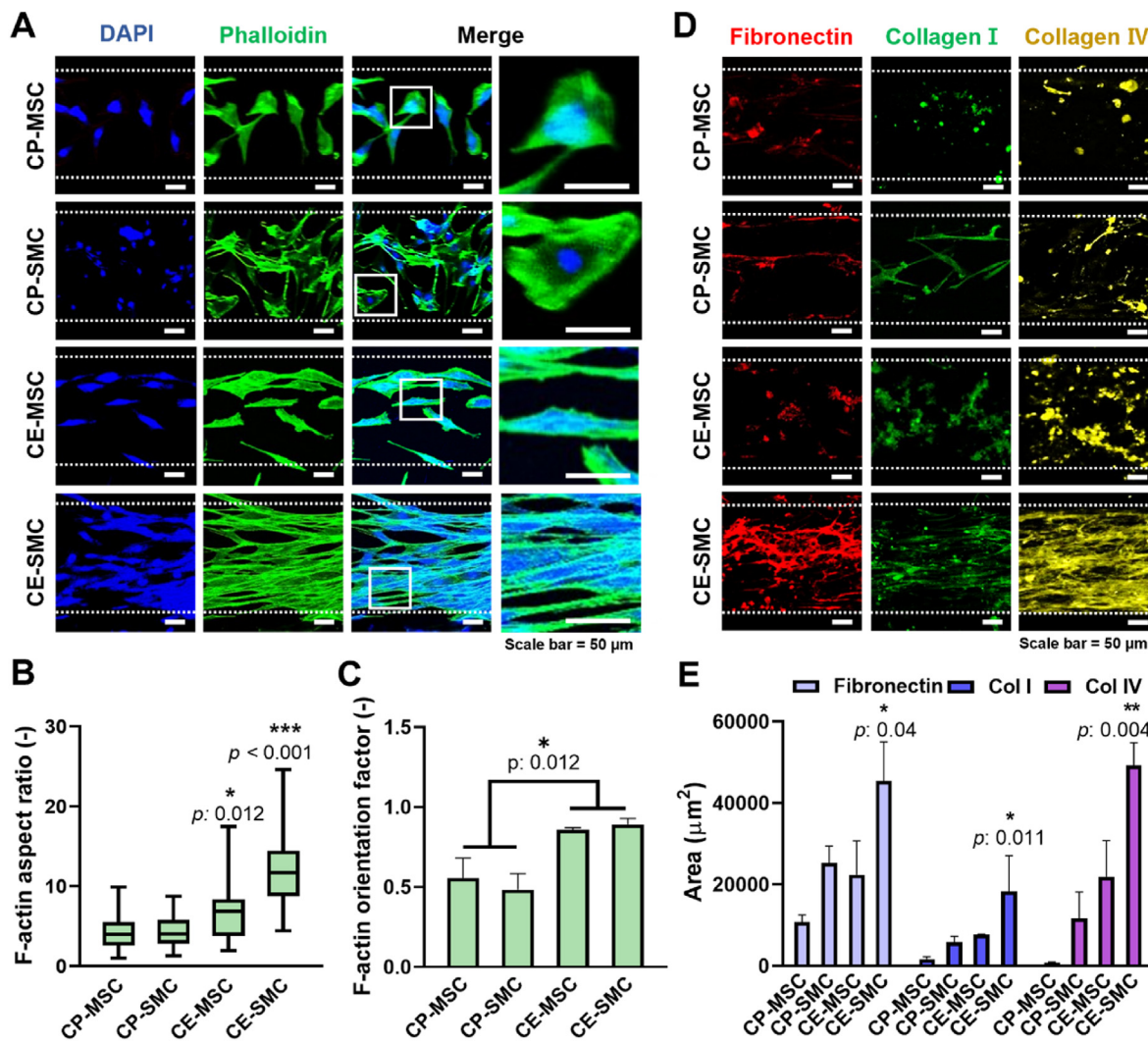


Fig. 3. Effects of cell printing (CP) and cell electrospraying (CE) on the arrangement of mesenchymal stem cells (MSCs) and stem cell-derived smooth muscle cells (SMCs). (a) Phalloidin/DAPI staining on day 21 and quantification of the (b) F-actin aspect ratio and (c) F-actin orientation factor. (d) Fluorescence images of fibronectin, collagen I, and collagen IV on day 21 and (e) quantification of area. Data indicate mean \pm SD ($n = 3$).

the tracheoesophageal tissue was dissected in the transverse direction (Fig. 5b (vi); left arrow, trachea; right arrow, esophagus).

Histological analysis of the esophageal tissues was performed using H&E and Masson's trichrome staining. Thick fibrotic tissues and increased infiltration of immune cells were observed in tissues transplanted with the control patch (Fig. 5c). In contrast, the esophagus transplanted with the CE-SMC patch exhibited a thick muscle layer and granulation tissue (Fig. 5d). To determine whether the transplanted patch promoted esophageal tissue regeneration, a detailed analysis was performed after immunostaining for vascular and smooth muscle markers (Fig. 6a, c). The number of ILB4⁺-SM22 α ⁺ blood vessels was higher in rats treated with the CE-SMC patch than in those treated with the control patch (Fig. 6e). Furthermore, the CE-SMC patch group exhibited abundant newly formed blood vessels, indicating that vascularization was promoted by the CE-SMC patch. Consequently, CE-SMC patch transplantation significantly increased the levels of SM22 α and vimentin relative to those in the control group (Fig. 6b, d). These data indicate higher esophageal muscle regeneration in the SMC-patch group than that in the control patch group. To confirm complete regeneration of esophageal epithelial cells, the esophageal specimens were stained with antibody against cytokeratin 14, a marker of squamous epithelial cells in the esophagus. The cytokeratin 14-positive esophageal epithelial cells covered the esophageal wounds of both control and SMC-patch groups

(Fig. S4), suggesting epithelial cell recruitment during wound healing.

To assess the effects of the CE-SMC patch on macrophage infiltration at the transplantation site, we performed CD68 immunostaining to identify macrophages (Fig. 7a). The number of macrophages in the transplanted tissue was significantly increased in rats with the control patch and decreased by 50% in the CE-SMC patch group (Fig. 7b). These results suggest that the CE-SMC patch attenuated the immune response during esophageal reconstruction.

4. Discussion

Cell alignment is critical for remodeling smooth muscle tissues, including the structure of the vasculature wall, intestinal tissue, and esophagus [50–52]; however, esophageal reconstruction by inducing SMC alignment has not been reported [53]. In this study, CE was proposed to guide cell alignment and elongation by generating aligned cell-laden micro/nanofibers. After CE, the electrospun MSCs and SMCs exhibited high cell viability, alignment, and elongation along the electrospun fibers. Moreover, CE induced uniaxially arranged F-actin and upregulated the expression levels of extracellular matrix proteins in MSCs and SMCs compared to 3D bioprinting. These results suggest that CE is a promising technique for manipulating cell elongation and alignment to mimic the anisotropic architecture of native tissues [54,55]. For

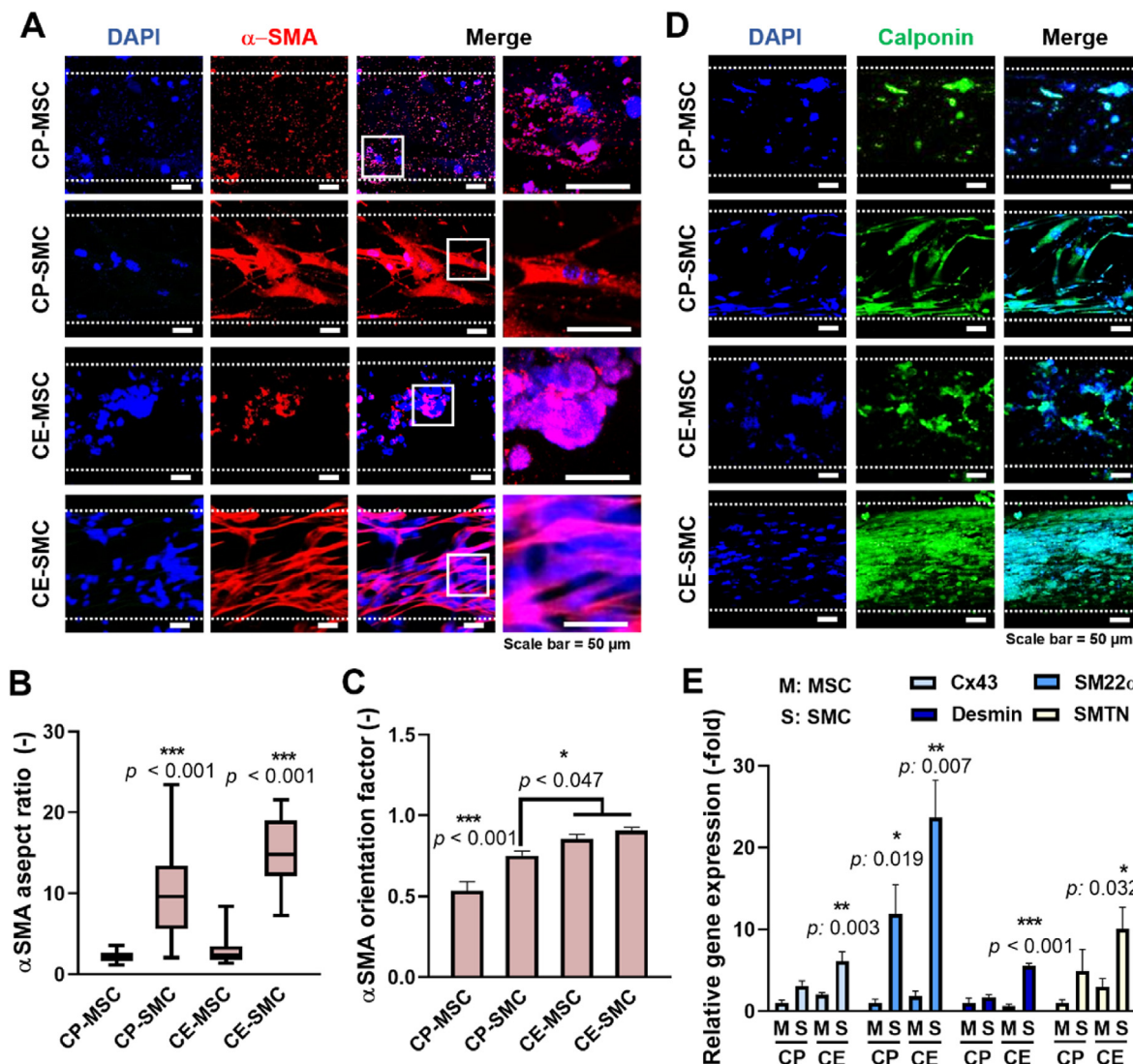


Fig. 4. Cell electrospinning (CE) promotes a higher degree of maturation of stem cell-derived smooth muscle cells (SMCs) than cell printing (CP). (a) α -SMA/DAPI staining on day 21 and quantification of the (b) alpha smooth muscle actin (α -SMA) aspect ratio and (c) α -SMA orientation factor. (d) Calponin/DAPI staining on day 21 and (e) analysis of relative smooth muscle-specific gene expression. GAPDH was used to normalize gene expression. Data indicate mean \pm SD ($n = 3$).

instance, when an “artificial wound” was covered with acellular electrospun fibers, SMCs successfully migrated to most of the wound area along the direction of the fibers [50]. These results suggest that a unidirectional microenvironment is favorable for developing an engineered smooth muscle patch that encourages efficient cell-cell interactions and an elongated morphology.

In addition, increased cytoskeletal and nuclear aspect ratios have been reported as critical factors in facilitating MSC-to-SMC differentiation, although the underlying mechanism by which biophysical microenvironments affect SMC differentiation is not clearly understood [56]. Cell elongation in parallel or perpendicular direction is important to SMCs in response to esophageal cycles for alleviating stress and prevent cellular damages [57]. This typical perpendicular direction of SMCs to strain was observed in esophageal tissues and named as hill-valley pattern in a number of studies [58–61]. Because of similarity to native esophageal structure and structural benefits, aligned nanofibrous scaffolds have usually shown superior cell alignment and proliferation than random nanofibrous scaffolds [62]. In this study, aligned nanofibrous layers were deposited in five layers in the horizontal and vertical directions, in which 10 cell layers (~300 μ m) will give similar thickness to native esophageal thickness (~270 μ m) [63]. However, SMC

differentiation was derived from various factors and verified from different aspects. Park et al. implanted randomly oriented PCL nanofibrous and 3D printed patches with and without seeding MSCs in rat esophagus [64]. Despite of preseeding MSCs, PCL nanofibrous patches revealed significantly increased esophagus thickness compared to 3D printed patches owing to the presence of topographic guidance. Hou et al. casted poly (ester urethane) scaffold using the silicon wafer with pattern prototype 1 (PU1; 200 μ m width and 30 μ m wide with 30 μ m depth wall) and 2 (PU2; 100 μ m width and discontinuous wall in 30 μ m gap for each 100 μ m channel with 30 μ m depth) [65]. Then, for implantation into rabbit esophagus, the scaffold was designed with PU1 on the exterior and PU2 on the interior to mimic endocircular and elongitunital architecture. Primary SMCs showed higher growth and differentiation rate compared to those on non-patterned scaffolds. Also, Kuppan et al. performed electrospinning for generating random and aligned fibrous scaffolds using PCL and PCL-gelatin blend. When SMCs were cultured on each scaffold, PCL-gelatin-aligned fibrous scaffolds revealed the highest cell proliferation and functional gene expression level. Here, cell proliferation was dependent on alignment, but gene expression levels were affected more by mechanical properties and chemical composition of scaffolds [66]. These former studies well support the findings of this

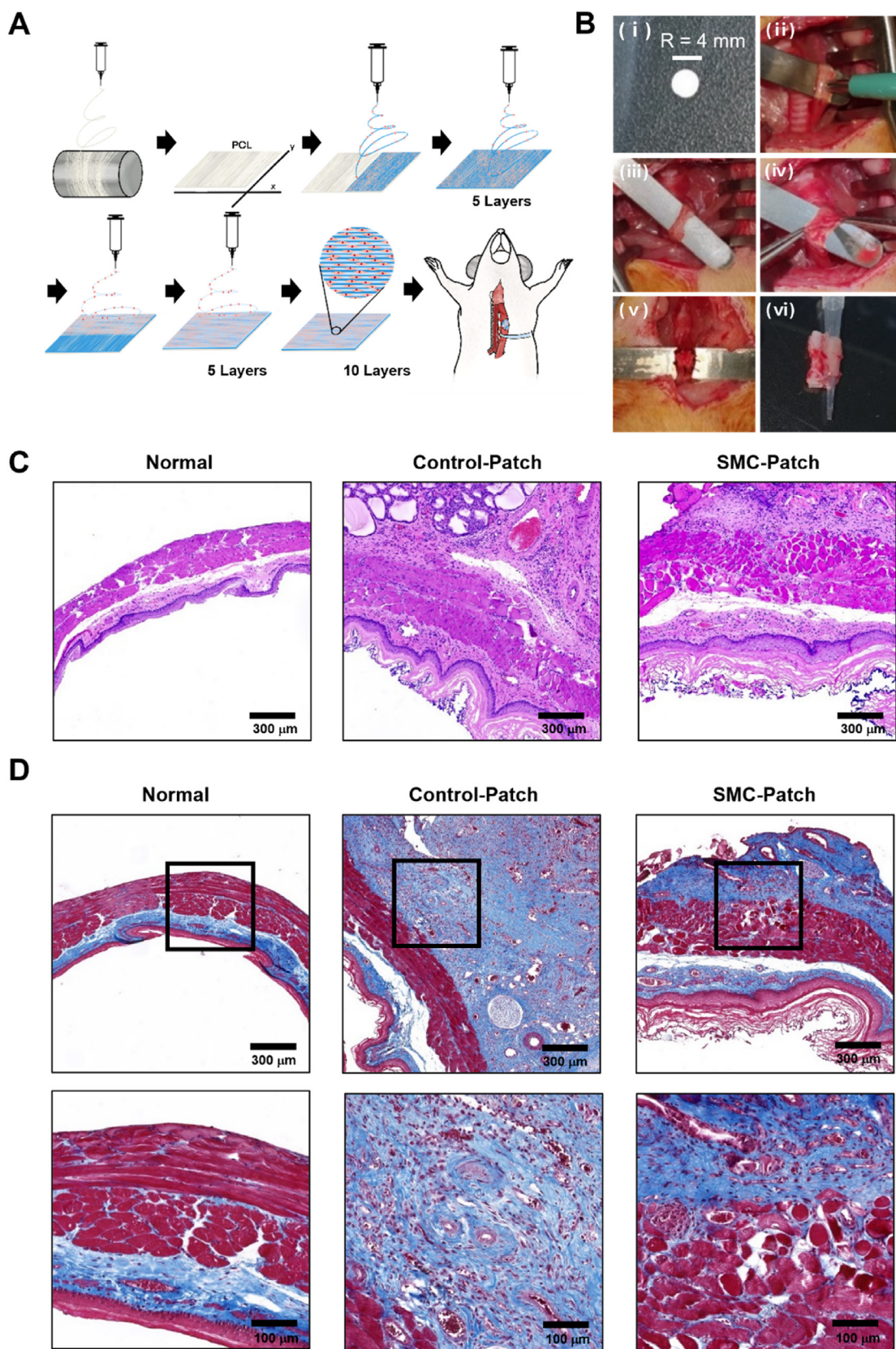


Fig. 5. Fabrication process and transplantation of a stem cell-derived smooth muscle cell (SMC)-patch to repair esophageal wound in a rat model. (a) Schematic illustration of polycaprolactone (PCL)-electrospinning and SMC-laden electrospinning for developing a cell electrospinning (CE)-SCM patch. (b) Representative images of the surgical procedure in which the CE-SCM patch was transplanted into the esophageal wound rat model. Images of (c) H&E staining and (d) Masson's trichrome staining of the defective esophagus at 2 weeks after transplantation of either an SMC or cell-free patch and normal esophagus. Representative data from two independent experiments are shown. (Normal, without surgery; Control-Patch, cell-free construct; SMC-Patch, SMC-laden construct).

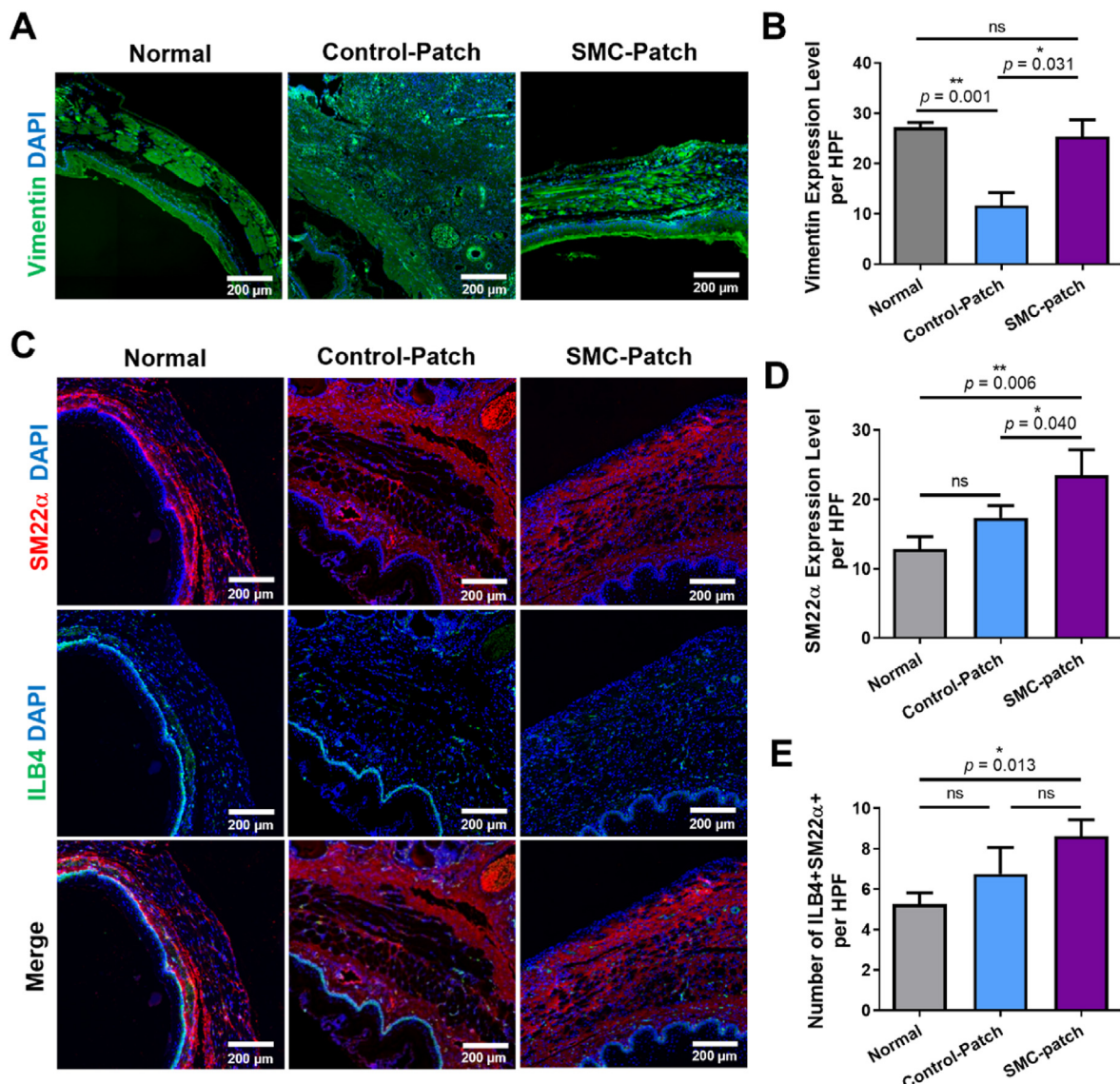


Fig. 6. Neovascularization and regeneration of esophageal smooth muscles after patch transplantation in an esophageal wound model. Representative images of (a) vimentin, (c) ILB4 and SM22 α immunostaining in an esophageal wound model at 2 weeks after transplantation of either a stem cell-derived smooth muscle cell (SMC) or cell-free patch and normal esophagus. Quantification of (b) vimentin and (d) SM22 α expression as measured by the fluorescence levels. (e) Quantification of the number of ILB4 and SM22 α double-positive cells. Data indicate mean \pm SD ($n = 6$). (Normal, without surgery; Control-Patch, cell-free construct; SMC-Patch, SMC-laden construct).

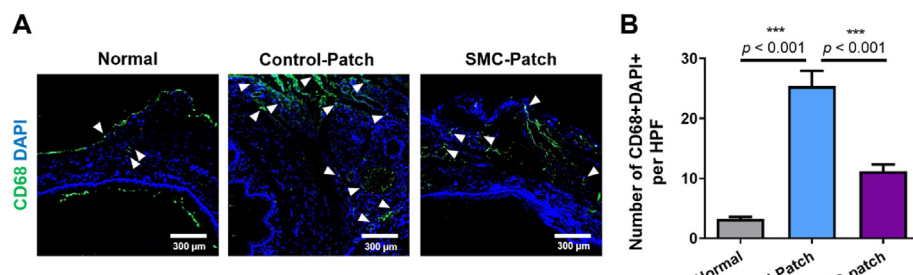


Fig. 7. Regulation of inflammation in esophageal tissues after stem cell-derived smooth muscle cell (SMC)-patch transplantation in an esophageal wound model. (a) Representative images of CD68 immunostaining in an esophageal wound model at 2 weeks after transplantation of either an SMC or cell-free patch and normal esophagus. (b) Quantification of macrophage infiltration in esophageal tissues by counting the number of DAPI and CD68 double-positive cells. Data indicate mean \pm SD ($n = 6$). (Normal, without surgery; Control-Patch, cell-free construct; SMC-Patch, SMC-laden construct).

study that the combination of aligned topography and TGF- β treatment significantly enhanced cell proliferation and SMC-specific gene expression.

In another aspect of SMC differentiation, MSCs have shown a greater

tendency to differentiate into SMCs on stiff substrates (90–1500 kPa) [67]. Hence, MSCs cultured on stiff substrates demonstrated increased calponin expression levels compared to MSCs cultured on soft substrates [43]. Additionally, the synergistic effects of a stiff surface and aligned

topographical cues can alter mechanical deformations (nuclear and cytoskeletal elongation) in cellular biochemical responses [68], which, in turn, can affect cellular functions and transcriptional activities [69]. In this study, alginate fibers exhibited a Young's modulus of 116 ± 3 kPa and a maximum strength of 3.5 ± 0.5 MPa. These results suggest that cells seeded on electrospun fibers preferentially differentiate into SMCs, owing to the appropriate mechanical properties and anisotropic cues. Moreover, CE-SMC exhibited an increased number of cells compared with the other groups. Although the molecular mechanisms involved in the increased proliferation of CE-SMC remain unclear, it is likely that aligned topographic cues may promote the proliferation of CE-SMCs.

TGF- β has been widely used to induce differentiation of MSCs into SMCs [70]. TGF- β -treated MSCs exhibit SMC-like phenotypes but may also become myoblast, adipogenic, or osteogenic cells depending on environmental factors [70,71]. Both α -SMA and calponin are key markers of an SMC-like population because α -SMA is expressed early in SMC development, whereas calponin is expressed exclusively in smooth muscle cells at the later stages of MSC-to-SMC differentiation. We found that α -SMA and calponin expression was dispersed in CP-SMC, but not all cells became SMCs. However, these proteins were highly expressed in CE-SMCs. In addition, the expression levels of contractile markers (CX43, SM22 α , desmin, and SMTN) were significantly increased in CE-SMCs in response to TGF- β , indicating that these cells were in the later stages of SMC differentiation [43,44].

As the esophageal tissue structure enables peristalsis, the contractile phenotype is a critical factor in assessing the potential to restore contraction and relaxation following esophageal injury. Our results indicate that a fibrous structure can serve not only as a mechanical support but also provide biophysical and biochemical cues. Esophageal injury can be caused by various factors, such as inflammation, ulcers, stenosis, cancer, or physical impact [72], and in severe cases, an injury can cause esophageal wounds. Small defects, perforation, and rupture of the esophagus are treated with sutures; however, if the defect is large, tissue transplantation is required. However, a practical method for effectively treating and regenerating the esophagus through tissue transplantation has not yet been developed. Consequently, many researchers have studied esophageal reconstruction through transplantation of tissue scaffolds made from MSCs [73–75]. In this study, we transplanted the CE-SMC patch into an esophageal wound model to evaluate its clinical applicability. Although the SMC scaffold was not transplanted into the esophagus in the form of a tube, but as a patch on a small wound area created by punching, we suggest an SMC-laden construct fabricated using CE as a useful method for esophageal reconstruction. In addition, PCL has long-term stability against biodegradation by hydrolysis, and it takes more than 2 years to completely degrade [76], implying the usefulness of PCL in CE-mediated tissue engineering. In H&E staining and cytokeratin 14 immunostaining, the esophagus has an inner mucosal layer and an outer muscular layer that are mainly composed of epithelium, suggesting recruitment of esophageal epithelial cells into the wounds. Although epithelial cells were not used for electrospinning in this study, the tissue transplantation and regenerative potential of the CE-SMC scaffolds were demonstrated. In future studies, we will aim to fabricate CE scaffolds using SMCs and epithelial cells for transplantation into small and large esophageal wounds to confirm functional tissue repair, potentially expanding the therapeutic and clinical significance of SMCs.

5. Conclusions

This study presents a novel approach to cell alignment and MSC-to-SMC differentiation via CE. Prior to CE, MSCs were treated with TGF- β as a regulatory factor of SMC differentiation, which efficiently yielded MSC-derived SMCs, as indicated by the enhanced expression levels of SMC-specific markers (calponin, α SMA, SM22 α , vimentin, desmin, and SMTN). Then, CE was performed using either MSCs or SMCs, and both cell types showed high cell viability ($>90\%$). CP using MSCs or SMCs was

compared as a control; specifically, electrospun SMCs (CE-SMCs) exhibited significantly elongated and aligned cytoskeletal structures represented by F-actin, fibronectin, collagen I, and collagen IV, which grew along the uniaxially deposited fiber direction. Additionally, the expression levels of SMC-specific markers (CX43, SM22 α , desmin, and SMTN) were significantly increased in CE-SMCs. When the CE-SMC scaffold was applied as a patch on a defective rat esophagus, an improved regenerative process was observed in terms of increased newly formed blood vessels and SM22 α and vimentin expression levels. These results suggest the potential of CE as a therapeutic approach for the regeneration of smooth muscle tissues.

Consent for publication

All authors have read and agreed to publish this manuscript.

Ethics approval and consent to participate

All animal experiments were reviewed and approved by the Institutional Review Board of the Pusan National University Hospital (PNUH-2021-188). Human palatine tonsil tissues were isolated from the patients after obtaining written informed consent. The study was approved by the Institutional Review Board of Pusan National University Hospital (1801-033-062).

Funding

This study was supported by the MRC program (NRF-2022R1A5A2027161) and grants from the National Research Foundation of Korea (NRF) funded by the Ministry of Science and ICT for the Bio-inspired Innovation Technology Development Project (NRF-2018M3C1B7021997) and the Korean Fund for Regenerative Medicine (KFRM) grant funded by the Ministry of Science and ICT, the Ministry of Health & Welfare (RS-2022-00070304), Republic of Korea.

Credit author statement

Miji Yeo: Conceptualization, Methodology, Investigation, Writing – original draft. Jung Won Yoon: Data curation, Formal analysis, Methodology, Writing – original draft. Gyu Tae Park: Data curation, Formal analysis, Methodology. Sung-Chan Shin: Formal analysis, Investigation, Methodology. Young-Cheol Song: Formal analysis, Investigation, Methodology. Yong-Il Cheon: Formal analysis, Investigation, Methodology. Byung-Joo Lee: Data curation, Formal analysis, Investigation. Geun Hyung Kim: Conceptualization, Funding acquisition, Methodology, Writing – review & editing, Supervision. Jae Ho Kim: Conceptualization, Funding acquisition, Methodology, Writing – review & editing, Supervision.

Declaration of competing interest

The authors declare that they have no known competing financial interests or personal relationships that could have appeared to influence the work reported in this paper.

Data availability

Data will be made available on request.

Acknowledgements

We would like to thank Yoon Ji Jung for technical assistance and Prof. Suck Won Hong (Pusan National University) for discussions that greatly improved the manuscript.

Appendix A. Supplementary data

Supplementary data to this article can be found online at <https://doi.org/10.1016/j.mtbio.2023.100564>.

Abbreviations

α -SMA	Alpha-smooth muscle actin
CE	Cell electrospinning
CP	Cell printing
DAPI	4',6-Diamidino-2-phenylindole
ECM	Extracellular matrix
MSCs	Mesenchymal stem cells
SMCs	Smooth muscle cells
TGF- β 1	Transforming growth factor- β 1

References

- [1] F. Schlottmann, M.G. Patti, Primary esophageal motility disorders: beyond achalasia, *Int. J. Mol. Sci.* 18 (7) (2017) 1399, <https://doi.org/10.3390/ijms18071399>.
- [2] R. Londono, S.F. Badylak, Regenerative medicine strategies for esophageal repair, *Tissue Eng. B Rev.* 21 (4) (2015) 393–410, <https://doi.org/10.1089/ten.teb.2015.0014>.
- [3] L. Arakelian, N. Kanai, K. Dua, M. Durand, P. Cattan, T. Ohki, Esophageal tissue engineering: from bench to bedside, *Ann. N. Y. Acad. Sci.* 1434 (1) (2018) 156–163, <https://doi.org/10.1111/nyas.13951>.
- [4] M.F. Pittenger, D.E. Discher, B.M. Peault, D.G. Phinney, J.M. Hare, A.I. Caplan, Mesenchymal stem cell perspective: cell biology to clinical progress, *NPJ Regen. Med.* 4 (1) (2019) 1–15, <https://doi.org/10.1038/s41536-019-0083-6>.
- [5] M.F. Pittenger, A.M. Mackay, S.C. Beck, R.K. Jaiswal, R. Douglas, J.D. Mosca, M.A. Moorman, D.W. Simonetti, S. Craig, D.R. Marshak, Multilineage potential of adult human mesenchymal stem cells, *Science* 284 (5411) (1999) 143–147, <https://doi.org/10.1126/science.284.5411.143>.
- [6] B. Ohlstein, T. Kai, E. Decotto, A. Spradling, The stem cell niche: theme and variations, *Curr. Opin. Cell Biol.* 16 (6) (2004) 693–699, <https://doi.org/10.1016/j.celb.2004.09.003>.
- [7] K. Kurpinski, H. Lam, J. Chu, A. Wang, A. Kim, E. Tsay, S. Agrawal, D.V. Schaffer, S. Li, Transforming growth factor-beta and notch signaling mediate stem cell differentiation into smooth muscle cells, *Stem Cell.* 28 (4) (2010) 734–742, <https://doi.org/10.1002/stem.319>.
- [8] S. Chen, R.J. Lechleider, Transforming growth factor-beta-induced differentiation of smooth muscle from a neural crest stem cell line, *Circ. Res.* 94 (9) (2004) 1195–1202, <https://doi.org/10.1161/01.RES.0000126897.41658.81>.
- [9] W.S. Park, S.C. Heo, E.S. Jeon, D.H. Hong, Y.K. Son, J.H. Ko, H.K. Kim, S.Y. Lee, J.H. Kim, J. Han, Functional expression of smooth muscle-specific ion channels in TGF-beta(1)-treated human adipose-derived mesenchymal stem cells, *Am. J. Physiol. Cell Physiol.* 305 (4) (2013) C377–C391, <https://doi.org/10.1152/ajpcell.00404.2012>.
- [10] C.Y. Tay, Y.L. Wu, P. Cai, N.S. Tan, S.S. Venkatraman, X. Chen, L.P. Tan, Bio-inspired micropatterned hydrogel to direct and deconstruct hierarchical processing of geometry-force signals by human mesenchymal stem cells during smooth muscle cell differentiation, *NPG Asia Mater.* 7 (7) (2015), [https://doi.org/10.1038/amt.2015.66 e199-e199](https://doi.org/10.1038/amt.2015.66).
- [11] A. Tijore, J.M. Behr, S.A. Irvine, V. Baisane, S. Venkatraman, Bioprinted gelatin hydrogel platform promotes smooth muscle cell contractile phenotype maintenance, *Biomed. Microdevices* 20 (2) (2018) 1–10, <https://doi.org/10.1007/s10544-018-0274-8>.
- [12] Q. Zhou, J. Xie, M. Bao, H. Yuan, Z. Ye, X. Lou, Y. Zhang, Engineering aligned electrospun PLLA microfibers with nano-porous surface nanotopography for modulating the responses of vascular smooth muscle cells, *J. Mater. Chem. B* (2015) 4439–4450, <https://doi.org/10.1039/C5TB00051C>.
- [13] A. Jiao, N.E. Trosper, H.S. Yang, J. Kim, J.H. Tsui, S.D. Frankel, C.E. Murry, D.H. Kim, Thermoresponsive nanofabricated substratum for the engineering of three-dimensional tissues with layer-by-layer architectural control, *ACS Nano* 8 (5) (2014) 4430–4439, <https://doi.org/10.1021/nn4063962>.
- [14] S.J. Kim, H.R. Cho, K.W. Cho, S. Qiao, J.S. Rhim, M. Soh, T. Kim, M.K. Choi, C. Choi, I. Park, N.S. Hwang, Multifunctional cell-culture platform for aligned cell sheet monitoring, transfer printing, and therapy, *ACS Nano* 9 (3) (2015) 2677–2688, <https://doi.org/10.1021/nn5064634>.
- [15] E. Ngandu Mpoyi, M. Cantini, P.M. Reynolds, N. Gadegaard, M.J. Dalby, M. Salmerón-Sánchez, Protein adsorption as a key mediator in the nanopographical control of cell behavior, *ACS Nano* 10 (7) (2016) 6638–6647, <https://doi.org/10.1021/acsnano.6b01649>.
- [16] A. Agrawal, B.H. Lee, S.A. Irvine, J. An, R. Bhuthalingam, V. Singh, K.Y. Low, C.K. Chua, S.S. Venkatraman, Smooth muscle cell alignment and phenotype control by melt spun polycaprolactone fibers for seeding of tissue engineered blood vessels, *Int. J. Biomater.* 2015 (2015), <https://doi.org/10.1155/2015/434876>.
- [17] J. Huang, Y. Chen, C. Tang, Y. Fei, H. Wu, D. Ruan, M.E. Paul, X. Chen, Z. Yin, B.C. Heng, W. Chen, The relationship between substrate topography and stem cell differentiation in the musculoskeletal system, *Cell. Mol. Life Sci.* 76 (3) (2019) 505–521, <https://doi.org/10.1007/s00018-018-2945-2>.
- [18] B.K.K. Teo, S.T. Wong, C.K. Lim, T.Y. Kung, C.H. Yap, Y. Ramagopal, L.H. Romer, E.K. Yim, Nanotopography modulates mechanotransduction of stem cells and induces differentiation through focal adhesion kinase, *ACS Nano* 7 (6) (2013) 4785–4798, <https://doi.org/10.1021/nn304966z>.
- [19] S. Jana, S.K. Levengood, M. Zhang, Anisotropic materials for skeletal-muscle-tissue engineering, *Adv. Mater.* 28 (48) (2016) 10588–10612, <https://doi.org/10.1002/adma.201600240>.
- [20] S.H. Cha, H.J. Lee, W.G. Koh, Study of myoblast differentiation using multi-dimensional scaffolds consisting of nano and micropatterns, *Biomater. Res.* 21 (1) (2017) 1–9, <https://doi.org/10.1186/s40824-016-0087-x>.
- [21] E.K. Yim, R.M. Reano, S.W. Pang, A.F. Yee, C.S. Chen, K.W. Leong, Nanopattern-induced changes in morphology and motility of smooth muscle cells, *Biomaterials* 26 (26) (2005) 5405–5413, <https://doi.org/10.1016/j.biomaterials.2005.01.058>.
- [22] A. Parandkh, A. Anbarlou, M. Tafazzoli-Shadpour, A. Ardeshirajimi, M.M. Khani, Substrate topography interacts with substrate stiffness and culture time to regulate mechanical properties and smooth muscle differentiation of mesenchymal stem cells, *Colloids Surf. B Biointerfaces* 173 (2019) 194–201, <https://doi.org/10.1016/j.colsurfb.2018.09.066>.
- [23] S. Abolhasani, M. Rajabizadeh, M.M. Khani, A. Parandkh, R. Hoseinpoor, The cooperative effects of micro-grooved topography and TGF-beta1 on the vascular smooth muscle cell contractile protein expression of the mesenchymal stem cells, *Differentiation* 115 (2020) 22–29, <https://doi.org/10.1016/j.diff.2020.06.003>.
- [24] X. Zhou, M. Nowicki, H. Sun, S.Y. Hann, H. Cui, T. Esworthy, J.D. Lee, M. Plemiak, L.G. Zhang, 3D Bioprinting-tunable small-diameter blood vessels with biomimetic biphasic cell layers, *ACS Appl. Mater. Interfaces* 12 (41) (2020) 45904–45915, <https://doi.org/10.1021/acsami.0c14871>.
- [25] H. Cui, W. Zhu, Y. Huang, C. Liu, Z.X. Yu, M. Nowicki, S. Miao, Y. Cheng, X. Zhou, S.J. Lee, Y. Zhou, In vitro and in vivo evaluation of 3D bioprinted small-diameter vasculature with smooth muscle and endothelium, *Biofabrication* 12 (1) (2019), 015004, <https://doi.org/10.1088/1758-5090/ab402c>.
- [26] J. Xue, T. Wu, Y. Dai, Y. Xia, Electrospinning and electrospun nanofibers: methods, materials, and applications, *Chem. Rev.* 119 (8) (2019) 5298–5415, <https://doi.org/10.1021/acs.chemrev.8b00593>.
- [27] C. Norioka, Y. Inamoto, C. Hajime, A. Kawamura, T. Miyata, A universal method to easily design tough and stretchable hydrogels, *NPG Asia Mater.* 13 (1) (2021) 1–10, <https://doi.org/10.1038/s41427-021-00302-2>.
- [28] S.L. Sampson, L. Saraiva, K. Gustafsson, S.N. Jayasinghe, B.D. Robertson, Cell electropinning: an in vitro and in vivo study, *Small* 10 (1) (2014) 78–82, <https://doi.org/10.1002/smll.201300804>.
- [29] E. Ehler, S.N. Jayasinghe, Cell electropinning cardiac patches for tissue engineering the heart, *Analyst* 139 (18) (2014) 4449–4452, <https://doi.org/10.1039/C4AN00766B>.
- [30] M. Yeo, G. Kim, Fabrication of cell-laden electrospun hybrid scaffolds of alginate-based bioink and PCL microstructures for tissue regeneration, *Chem. Eng. J.* 275 (2015) 27–35, <https://doi.org/10.1016/j.cej.2015.04.038>.
- [31] H. Chen, Y. Liu, Q. Hu, A novel bioactive membrane by cell electropinning, *Exp. Cell Res.* 338 (2) (2015) 261–266, <https://doi.org/10.1016/j.yexcr.2015.08.007>.
- [32] M. Yeo, G. Kim, Anisotropically aligned cell-laden nanofibrous bundle fabricated via cell electropinning to regenerate skeletal muscle tissue, *Small* 14 (48) (2018), 1803491, <https://doi.org/10.1002/smll.201803491>.
- [33] M. Yeo, G. Kim, Micro/nano-hierarchical scaffold fabricated using a cell electropinning/3D printing process for co-culturing myoblasts and HUVECs to induce myoblast alignment and differentiation, *Acta Biomater.* 107 (2020) 102–114, <https://doi.org/10.1016/j.actbio.2020.02.042>.
- [34] M. Zhuravleva, Z. Gilazieva, T.E. Grigoriev, A.D. Shepelev, T. Kh Tenchurin, R. Kamyshinsky, S.V. Krasheninnikov, S. Orlov, G. Caralogli, S. Archipova, M.J. Holterman, In vitro assessment of electrospun polyamide-6 scaffolds for esophageal tissue engineering, *J. Biomed. Mater. Res. Part B Appl. Biomater.* 107 (2) (2019) 253–268, <https://doi.org/10.1002/jbm.b.34116>.
- [35] B. Wu, N. Takeshita, Y. Wu, S. Vijayaventakaraman, K.Y. Ho, W.F. Lu, J.Y.H. Fuh, Pluronic F127 blended polycaprolactone scaffolds via e-jetting for esophageal tissue engineering, *J. Mater. Sci. Mater. Med.* 29 (9) (2018) 1–12, <https://doi.org/10.1007/s10856-018-6148-z>.
- [36] S.C. Shin, Y. Seo, H.Y. Park, D.W. Jung, T.H. Shin, H. Son, Y.K. Kim, J.C. Lee, E.S. Sung, J.Y. Jang, H.S. Kim, Regenerative potential of tonsil mesenchymal stem cells on surgical cutaneous defect, *Cell Death Dis.* 9 (2) (2018) 1–12, <https://doi.org/10.1038/s41419-017-0248-4>.
- [37] G.C. Park, J.S. Song, H.Y. Park, S.C. Shin, J.Y. Jang, J.C. Lee, S.G. Wang, B.J. Lee, J.S. Jung, Role of fibroblast growth factor-5 on the proliferation of human tonsil-derived mesenchymal stem cells, *Stem Cell. Dev.* 25 (15) (2016) 1149–1160, <https://doi.org/10.1089/scd.2016.0061>.
- [38] J. Brun, K.A. Lutz, K.M. Neumayer, G. Klein, T. Seeger, T. Uynuk-Ool, K. Wörgötter, S. Schmid, U. Kraushaar, E. Guenther, B. Rolauffs, Smooth muscle-like cells generated from human mesenchymal stromal cells display marker gene expression and electrophysiological competence comparable to bladder smooth muscle cells, *PLoS One* 10 (12) (2015), e0145153, <https://doi.org/10.1371/journal.pone.0145153>.
- [39] S. Chang, S. Song, J. Lee, J. Yoon, J. Park, S. Choi, J.K. Park, K. Choi, C. Choi, Phenotypic modulation of primary vascular smooth muscle cells by short-term culture on micropatterned substrate, *PLoS One* 9 (2) (2014), e88089, <https://doi.org/10.1371/journal.pone.0088089>.
- [40] G. Kim, K.E. Park, Alginate-nanofibers fabricated by an electrohydrodynamic process, *Polym. Eng. Sci.* 49 (11) (2009) 2242–2248, <https://doi.org/10.1002/pen.21472>.

- [41] C.A. Bonino, M.D. Krebs, C.D. Saquing, S.I. Jeong, K.L. Shearer, E. Alsberg, S.A. Khan, Electrospinning alginate-based nanofibers: from blends to crosslinked low molecular weight alginate-only systems, *Carbohydr. Polym.* 85 (1) (2011) 111–119, <https://doi.org/10.1016/j.carbpol.2011.02.002>.
- [42] S. Huang, P. Chen, X. Shui, Y. He, H. Wang, J. Zheng, L. Zhang, J. Li, Y. Xue, C. Chen, W. Lei, Baicalin attenuates transforming growth factor- β 1-induced human pulmonary artery smooth muscle cell proliferation and phenotypic switch by inhibiting hypoxia inducible factor-1 α and aryl hydrocarbon receptor expression, *J. Pharm. Pharmacol.* 66 (10) (2014) 1469–1477, <https://doi.org/10.1111/jphb.12273>.
- [43] A.P. Rickel, H.J. Sanyour, N.A. Leyda, Z. Hong, Extracellular matrix proteins and substrate stiffness synergistically regulate vascular smooth muscle cell migration and cortical cytoskeleton organization, *ACS Appl. Bio Mater.* 3 (4) (2020) 2360–2369, <https://doi.org/10.1021/acsabm.0c00100>.
- [44] J.S. Weinbaum, J. Qi, R.T. Tranquillo, Monitoring collagen transcription by vascular smooth muscle cells in fibrin-based tissue constructs, *Tissue Eng. C Methods* 16 (3) (2010) 459–467, <https://doi.org/10.1089/ten.tec.2009.0112>.
- [45] J. Wang, R. Zohar, C.A. McCulloch, Multiple roles of α -smooth muscle actin in mechanotransduction, *Exp. Cell Res.* 312 (3) (2006) 205–214, <https://doi.org/10.1016/j.yexcr.2005.11.004>.
- [46] S. Soliman, S. Sant, J.W. Nichol, M. Khabiry, E. Traversa, A. Khademhosseini, Controlling the porosity of fibrous scaffolds by modulating the fiber diameter and packing density, *J. Biomed. Mater. Res., Part A* 96 (3) (2011) 566–574, <https://doi.org/10.1002/jbm.a.33010>.
- [47] L. Moroni, R. Licht, J. de Boer, J.R. de Wijn, C.A. van Blitterswijk, Fiber diameter and texture of electrospun PEOT/PBT scaffolds influence human mesenchymal stem cell proliferation and morphology, and the release of incorporated compounds, *Biomaterials* 27 (28) (2006) 4911–4922, <https://doi.org/10.1016/j.biomaterials.2006.05.027>.
- [48] C.A. Bashur, L.A. Dahlgren, A.S. Goldstein, Effect of fiber diameter and orientation on fibroblast morphology and proliferation on electrospun poly (D, L-lactic-co-glycolic acid) meshes, *Biomaterials* 27 (33) (2006) 5681–5688, <https://doi.org/10.1016/j.biomaterials.2006.07.005>.
- [49] P. Maghsoudlou, S. Eaton, P. De Coppi, *Tissue engineering of the esophagus*, in: *Seminars in Pediatric Surgery*, Elsevier, Philadelphia, 2014, pp. 127–134.
- [50] B. Yi, Y. Shen, H. Tang, X. Wang, B. Li, Y. Zhang, Stiffness of aligned fibers regulates the phenotypic expression of vascular smooth muscle cells, *ACS Appl. Mater. Interfaces* 7 (2019) 6867–6880, <https://doi.org/10.1021/acsmami.9b00293>.
- [51] Y. Chen, C. Guo, E. Manousiouthakis, X. Wang, D.M. Cairns, T.T. Roh, C. Du, D.L. Kaplan, Bi-layered tubular microfiber scaffolds as functional templates for engineering human intestinal smooth muscle tissue, *Adv. Funct. Mater.* 30 (17) (2020), 2000543, <https://doi.org/10.1002/adfm.202000543>.
- [52] E.J. Chung, H.W. Ju, Y.K. Yeon, J.S. Lee, Y.J. Lee, Y.B. Seo, P. Chan Hum, Development of an omentum-cultured oesophageal scaffold reinforced by a 3D-printed ring: feasibility of an *in vivo* bioreactor, *Artif. Cell Nanomed. Biotechnol.* 46 (sup1) (2018) 885–895, <https://doi.org/10.1080/21691401.2018.1439039>.
- [53] S.Y. Park, J.W. Choi, J.K. Park, E.H. Song, S.A. Park, Y.S. Kim, Y.S. Shin, C.H. Kim, Tissue-engineered artificial oesophagus patch using three-dimensionally printed polycaprolactone with mesenchymal stem cells: a preliminary report, *Interact. Cardiovasc. Thorac. Surg.* 22 (6) (2016) 712–717, <https://doi.org/10.1093/icvts/ivw048>.
- [54] R.G. Thakar, Q. Cheng, S. Patel, J. Chu, M. Nasir, D. Liepmann, K. Komvopoulos, S. Li, Cell-shape regulation of smooth muscle cell proliferation, *Biophys. J.* 96 (8) (2009) 3423–3432, <https://doi.org/10.1016/j.bpj.2008.11.074>.
- [55] E.K. Yim, R.M. Reano, S.W. Pang, A.F. Yee, C.S. Chen, K.W. Leong, Nanopattern-induced changes in morphology and motility of smooth muscle cells, *Biomaterials* 26 (26) (2005) 5405–5413, <https://doi.org/10.1016/j.biomat.2005.01.058>.
- [56] Y.T. Yeh, J. Wei, S. Thorossian, K. Nguyen, C. Hoffman, J.C. Del Álamo, R. Serrano, Y.S.J. Li, K.C. Wang, S. Chien, MiR-145 mediates cell morphology-regulated mesenchymal stem cell differentiation to smooth muscle cells, *Biomaterials* 204 (2019) 59–69, <https://doi.org/10.1016/j.biomat.2019.03.003>.
- [57] A.C. Ritchie, S. Wijaya, W.F. Ong, S.P. Zhong, K.S. Chian, Dependence of alignment direction on magnitude of strain in esophageal smooth muscle cells, *Biotechnol. Bioeng.* 102 (6) (2009) 1703–1711, <https://doi.org/10.1002/bit.22190>.
- [58] J.M. Cha, S.N. Park, S.H. Noh, H. Suh, Time-dependent modulation of alignment and differentiation of smooth muscle cells seeded on a porous substrate undergoing cyclic mechanical strain, *Artif. Organs* 30 (4) (2006) 250–258, <https://doi.org/10.1111/j.1525-1594.2006.00212.x>.
- [59] J.H. Haga, Y.-S.J. Li, S. Chien, Molecular basis of the effects of mechanical stretch on vascular smooth muscle cells, *J. Biomech.* 40 (5) (2007) 947–960, <https://doi.org/10.1016/j.jbiomech.2006.04.011>.
- [60] K. Hayakawa, N. Sato, T. Obinata, Dynamic reorientation of cultured cells and stress fibers under mechanical stress from periodic stretching, *Exp. Cell Res.* 268 (1) (2001) 104–114.
- [61] K. Kanda, T. Matsuda, T. Oka, Mechanical stress induced cellular orientation and phenotypic modulation of 3-D cultured smooth muscle cells, *Am. Soc. Artif. Intern. Organs J.* 39 (3) (1993) M686–M690.
- [62] A. Subramanian, U.M. Krishnan, S. Sethuraman, Fabrication, characterization and *in vitro* evaluation of aligned PLGA-PCL nanofibers for neural regeneration, *Ann. Biomed. Eng.* 40 (10) (2012) 2098–2110, <https://doi.org/10.1007/s10439-012-0592-6>.
- [63] B.E. Bouma, G.J. Tearney, C.C. Compton, N.S. Nishioka, High-resolution imaging of the human esophagus and stomach *in vivo* using optical coherence tomography, *Gastrointest. Endosc.* 51 (4) (2000) 467–474, [https://doi.org/10.1016/S0016-5107\(00\)70449-4](https://doi.org/10.1016/S0016-5107(00)70449-4).
- [64] H. Park, I.G. Kim, Y. Wu, H. Cho, J.W. Shin, S.A. Park, E.J. Chung, Experimental investigation of esophageal reconstruction with electrospun polyurethane nanofiber and 3D printing polycaprolactone scaffolds using a rat model, *Head Neck* 43 (3) (2021) 833–848, <https://doi.org/10.1002/hed.26540>.
- [65] L. Hou, C. Gong, Y. Zhu, In vitro construction and *in vivo* regeneration of esophageal bilamellar muscle tissue, *J. Biomater. Appl.* 30 (9) (2016) 1373–1384, <https://doi.org/10.1177/0885328215627585>.
- [66] P. Kuppan, S. Sethuraman, U.M. Krishnan, Interaction of human smooth muscle cells with nanofibrous scaffolds: effect of fiber orientation on cell adhesion, proliferation, and functional gene expression, *J. Biomed. Mater. Res., Part A* 103 (7) (2015) 2236–2250, <https://doi.org/10.1002/jbm.a.35360>.
- [67] J.S. Park, J.S. Chu, A.D. Tsou, R. Diop, Z. Tang, A. Wang, S. Li, The effect of matrix stiffness on the differentiation of mesenchymal stem cells in response to TGF- β , *Biomaterials* 32 (16) (2011) 3921–3930, <https://doi.org/10.1016/j.biomaterials.2011.02.019>.
- [68] D.E. Ingber, Tensegrity: the architectural basis of cellular mechanotransduction, *Annu. Rev. Physiol.* 59 (1) (1997) 575–599, <https://doi.org/10.1146/annurev.physiol.59.1.575>.
- [69] N. Wang, J.D. Tytell, D.E. Ingber, Mechanotransduction at a distance: mechanically coupling the extracellular matrix with the nucleus, *Nat. Rev. Mol. Cell Biol.* 10 (1) (2009) 75–82, <https://doi.org/10.1038/nrm2594>.
- [70] Y. Liu, B. Deng, Y. Zhao, S. Xie, R. Nie, Differentiated markers in undifferentiated cells: expression of smooth muscle contractile proteins in multipotent bone marrow mesenchymal stem cells, *Dev. Growth Differ.* 55 (5) (2013) 591–605, <https://doi.org/10.1111/dgd.12052>.
- [71] N.P. Talele, J. Fradette, J.E. Davies, A. Kapus, B. Hinz, Expression of α -smooth muscle actin determines the fate of mesenchymal stromal cells, *Stem Cell Rep.* 4 (6) (2015) 1016–1030.
- [72] J.B. Zwischenberger, C. Savage, A. Bidani, Surgical aspects of esophageal disease: perforation and caustic injury, *Am. J. Respir. Crit. Care Med.* 165 (8) (2002) 1037–1040, <https://doi.org/10.1161/01.res.2015.05.004>.
- [73] J. Catry, M. Luong-Nguyen, L. Arakelian, T. Poghosyan, P. Bruneval, T. Domet, L. Michaud, R. Sfeir, F. Gottrand, J. Larghero, V. Vanneaux, Circumferential esophageal replacement by a tissue-engineered substitute using mesenchymal stem cells: an experimental study in mini pigs, *Cell Transplant.* 26 (12) (2017) 1831–1839, <https://doi.org/10.1177/0963689717741498>.
- [74] H. Park, I.G. Kim, Y. Wu, H. Cho, J.W. Shin, S.A. Park, E.J. Chung, Experimental investigation of esophageal reconstruction with electrospun polyurethane nanofiber and 3D printing polycaprolactone scaffolds using a rat model, *Head Neck* 43 (3) (2021) 833–848, <https://doi.org/10.1002/hed.26540>.
- [75] I.G. Kim, Y. Wu, S.A. Park, H. Cho, J.J. Choi, S.K. Kwon, J.W. Shin, E.J. Chung, Tissue-engineered esophagus via bioreactor cultivation for circumferential esophageal reconstruction, *Tissue Eng.* 25 (21–22) (2019) 1478–1492, <https://doi.org/10.1089/ten.tea.2018.0277>.
- [76] S. Sanchez-Gonzalez, N. Diban, A. Urtiaga, Hydrolytic degradation and mechanical stability of poly(epsilon-caprolactone)/reduced graphene oxide membranes as scaffolds for *in vitro* neural tissue regeneration, *Membranes* 8 (1) (2018) 12, <https://doi.org/10.3390/membranes8010012>.